Taylor & Francis
Taylor & Francis Group

A graph-based approach for assessing storm-induced coastal changes

Qiusheng Wu [a], Haibin Su[b], Douglas J. Sherman[c], Hongxing Liu[d], Jennifer M. Wozencraft[e], Bailang Yu [f,g] and Zuoqi Chen[f,g]

aDepartment of Geography, Binghamton University, State University of New York, Binghamton, NY, USA; bDepartment of Physics and Geosciences, Texas A&M University-Kingsville, Kingsville, TX, USA; cDepartment of Geography, University of Alabama, Tuscaloosa, AL, USA; dDepartment of Geography, University of Cincinnati, Cincinnati, OH, USA; eUS Army Corp of Engineers, Kiln, MS, USA; fKey Laboratory of Geographic Information Science, Ministry of Education, East China Normal University, Shanghai, China; gSchool of Geographic Sciences, East China Normal University, Shanghai, China

ABSTRACT

Hurricanes and tropical storms are severe threats to coastal properties, settlements, and infrastructure. Airborne light detection and ranging (lidar) surveys conducted before and after storm events allow detailed analysis of coastal geomorphologic and sediment volumetric changes and have been proved very useful in the study of coastal changes. Traditionally, most studies use the pixel-based differencing method to quantify the spatial extent and magnitude of coastal changes based on sequential lidar surveys. This research presents a graph theory-based approach and associated software tools for representing and quantifying storm-induced damages to buildings, beaches and sand dunes, coastal vegetation canopy, and infrastructure. Generation of elevation difference grids, construction of local contour trees, and derivation of semantic properties are key components of the new algorithm for change object detection and extraction. An ontology and taxonomy are proposed to classify change objects into different types of coastal damages in terms of their semantic properties. This method has been successfully applied to assess damages of Hurricane Ike to the Bolivar Peninsula on the Texas Gulf Coast based on pre- and post-storm airborne lidar data and colour infrared aerial photographs.

1. Introduction

Hurricanes and tropical storms are severe threats to coastal properties, settlements, and infrastructure (Trepanier et al. 2015). According to NOAA's National Coastal Population Report (NOAA 2013), more than 123 million people, i.e. 39% of the U.S. population, are concentrated in coastal shoreline counties, which account for less than 10% of the total U.S. continental land area. With the increasing number of people moving into coastal zones, more and more buildings and infrastructure have been built, increasing both demand for coastal resources and vulnerability of those resources. With the increase in coastal developments, future hurricanes and tropical storms are likely to cause greater

---

CONTACT Qiusheng Wu ✉ wqs@binghamton.edu 🖃 Department of Geography, Binghamton University, State University of New York, Binghamton, NY 13902, USA

economic damages. Managing for coastal hazards is an important component of rational decision-making in order to mitigate economic losses. Understanding the impacts of previous storms is important for estimating future damages.

Airborne light detection and ranging (lidar) has been used as a reliable method of gathering highly accurate and densely sampled topographic data (White and Wang 2003; Liu et al. 2011; Wu, Lane, and Liu 2014; Yu et al. 2010; Wu, Deng, and Chen 2016). Airborne lidar surveys conducted before and after storm events allow detailed analysis of coastal geomorphologic and sediment volumetric changes and have been proven very useful in the study of coastal changes (Finkl, Benedet, and Andrews 2005; Zhang et al. 2005; Sallenger et al. 2006; Robertson, Zhang, and Whitman 2007; Liu et al. 2010; Sherman et al. 2013; Wozencraft and Lillycrop 2003; Houser and Hamilton 2009; Rogers et al. 2015; Gens 2010). Traditionally, most studies use the pixel-based differencing method to quantify the spatial extent and magnitude of coastal changes based on sequential lidar surveys (Sallenger et al. 2003; White and Wang 2003; Zhang et al. 2005; Doran et al. 2009; Hardin et al. 2014b). With the pixel-based differencing method, morphological and volumetric changes are calculated by differencing the post-event lidar digital elevation model (DEM) to the pre-event lidar DEM on each grid cell. The total volume of deposition can then be computed by summing all positive values in the elevation difference grid. Similarly, the total volume of erosion is computed by summing all negative values in the elevation difference grid. The net volume change is defined by the difference between total deposition volume and total erosion volume. The traditional approach can only derive the overall total change of the study area, but analysis of spatial patterns of morphological change still relies on the visual interpretation of the elevation difference grid. Because the traditional method only calculates the total volume of deposition, erosion, and net change for a study area, it is unable to represent and quantify surface elevation and volume changes for deposition or erosion patches at a local scale unless the study area is partitioned into smaller sections. Nevertheless, spatial variations within those sections cannot be discerned automatically.

This research presents an object and graph theory-based approach and associated software tools for representing and quantifying hurricane (or other storm)-induced damages to buildings, beaches and sand dunes, coastal vegetation canopy, and infrastructure. A localized contour tree algorithm (Wu et al. 2015) based on graph theory (Phillips, Schwanghart, and Heckmann 2015; Heckmann, Schwanghart, and Phillips 2015) has been developed to detect and extract surface change objects that can be related to specific landscape features, using repeat topographic lidar data. To the best of our knowledge, no studies utilizing graph theory for coastal change analysis have been reported. Our proposed method explicitly represents surface morphological changes as individual change objects (patches). A set of quantitative attributes is derived from these change objects as the basis for assessing the extent, nature, and magnitude of coastal damages caused by a storm event. We applied this method to assessing the Hurricane Ike damages to the Bolivar Peninsula on the Texas Gulf Coast based on pre- and post-storm airborne lidar data and colour infrared (CIR) aerial photographs.

2. Object and graph theory based analytical framework

Natural hazards could do substantial damage to the landscape. Damage to resources of interest is typically reflected in such changes. Therefore, some physical aspects of

damage assessment can be performed by detecting and quantifying landscape change. Both field data model and object data model in geographical information science can be used to represent landscape changes (Goodchild 1992; Fonseca, Davis, and Camara 2003; Liu et al. 2008).

The field model represents changes as a smooth, continuous field of elevation variations across geographical space. The object model represents the changes as discrete, identifiable change entities (patches), which can be described by various geometric and shape attributes. In previous coastal hazard studies with repeat lidar surveys, coastal changes and associated damages were commonly represented and evaluated based on the field model (Zhang et al. 2005; Doran et al. 2009; Hardin et al. 2014b). Human analysts visually interpreted the elevation difference grid and perceptually organized the elevation cells into various erosion and deposition objects (patches) in order to gain a higher level of information and knowledge for a qualitative assessment of the spatial distribution of changes. The large volume of elevation difference values does not carry much explicit high-level information or knowledge about the nature and magnitude of damage for assessing some critical issues, such as the number of buildings destroyed, the quantity of sediment eroded from a particular beach geomorphological element (e.g. foreshore, backshore, or dune), or the alongshore locations of erosion hot spots.

This study adopts an object-based, conceptual framework for change detection and damage assessment. With this framework, we represent storm-induced changes to buildings, coastal facilities, trees, and patches of sediment erosion or deposition as a series of discrete and identifiable, geo-referenced objects. Various geometric, shape, volumetric as well as spectral attributes can be derived to characterize these objects for automated recognition and assessment of different types of coastal damages. The object data model extracts the essential change and damage information while discarding irrelevant and unimportant details in massive lidar data sets. It overcomes the well-known salt-and-pepper effect (Blaschke 2010; Kim et al. 2011; Blaschke et al. 2014). For example, some 'isolated' pixels in the elevation difference grid caused by lidar data noise can be effectively removed. These change objects, rather than individual grid cells, are used as basic spatial units for subsequent damage classification and analysis. An ontology-driven taxonomy (Agarwal 2005; Fonseca, Davis, and Camara 2003; Couclelis 2010) is established for cognitive use of *a priori* knowledge to interpret and classify change objects into different categories of damage (Figure 1). The domain of ontology comprehends objects, relations, boundaries, events, processes, qualities, and quantities of all sorts (Mark, Smith, and Tversky 1999). Our focus here is on the domain of geographic objects in the narrow sense, which comprehends regions such as building, trees, grass, beach sediments, etc. Geographic objects are spatial objects on or near the earth surface and they have boundaries. In terms of boundary characteristics, geographic objects can be divided into two types: bona fide objects and fiat objects (1999). Bona fide objects are associated with buildings and other man-made structures, which have determinate and prominent boundaries that enclose them and separate them from their backgrounds. Fiat objects are associated with beaches, sand dunes, and vegetation canopy, which have vaguely defined boundaries and are created by spatial analysis and human cognition. To organize knowledge in terms of cognitive categories, a tree-structure taxonomy is constructed with general categories at the higher level, while specific categories are used at the lower level. Category classes in the geographic domain
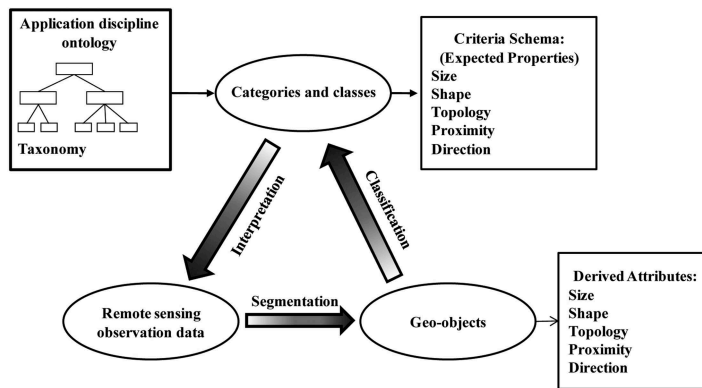
Figure 1. The ontology-driven taxonomy.

manifest certain spatial features that reflect specific ontological characteristics of geographic objects. There is a group of properties characteristic of a category that typical members of that category are likely to have. For example, buildings usually have regular geometric shapes and high relief relative to a background, while sediment patches have irregular and fractal shape and relatively low relief. The statistical characteristics of the samples of each category can be used as the basis of classifying the change objects.

In this study, high-resolution aerial photographs and high-resolution DEMs derived from airborne lidar data were used to delineate boundaries of geographic objects using the graph-based localized contour tree algorithm (Wu et al. 2015). Details about the used data are provided in the case study section. Various geometric and shape attributes were calculated to quantify the geographic objects. By analysing the relationship between expected properties and derived attributes, a rule-based classification method is proposed to classify the geographic objects into different categories.

The ontology for coastal damage assessment is a formal representation of a set of damage categories, the relationships between these categories, and the expected semantic properties associated with each category. As shown in Figure 2, the damage categories are arranged in a taxonomic hierarchy, which include super-ordinate categories and more specific subordinate categories that inherit their super-ordinate's properties. Each damage category has a set of expected properties associated with it that allow us to recognize change objects belonging to that specific category. Based on our prior knowledge, the hurricane-induced coastal damage is conceptualized into four categories: building damage; vegetation damage; beach and dune damage; and infrastructure damage (Reif et al. 2013). The damage to buildings and infrastructure can be detected and evaluated by the change objects associated with their destruction, collapse, and relocation as a consequence of hurricane winds and waves, and storm surge. The damage to beaches and sand dunes is represented by change patches/objects and associated sediment erosion and deposition. The vegetation damage is assessed by destruction and stresses of trees and grasses. The change objects associated with building damage, vegetation damage, beach and dune damage, and infrastructure damage each has some distinct properties (Figure 2). For instance, change objects associated with building damage often have a compact
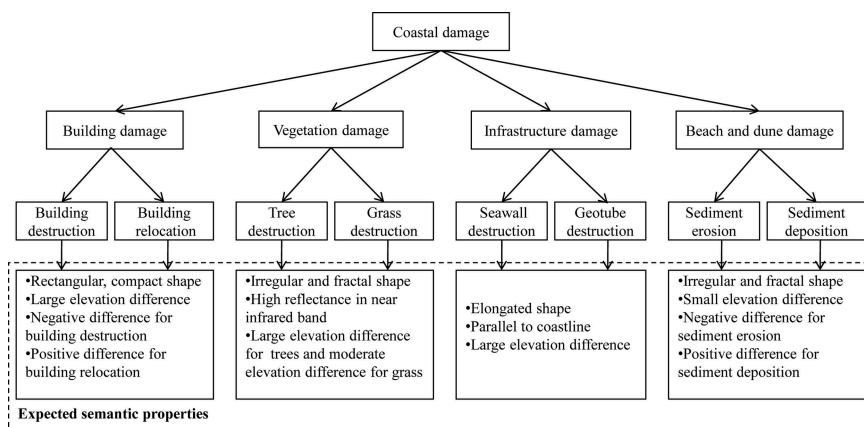
Figure 2. Taxonomic hierarchy of damage categories.

shape and a large elevation difference, and change objects associated with the beach and dune damage tend to have an irregular and fractal shape as well as smaller and gradually changing elevation difference in comparison to change objects associated with building damage.

The expected semantic properties and semantic relations of the damage categories in the taxonomy provide the ontological basis for formulating a set of criteria to recognize and classify change objects into different damage categories. A rule-based approach is used in this study to represent the expected properties and relations (criteria) of a category. The combined use of change objects and an ontology-driven taxonomy provides a formal analytical framework for classifying and quantifying hurricane-induced coastal damages.

3. Numerical algorithms for change object extraction and attribution

Before a change object can be measured, interpreted, and classified, it must first be identified and delineated. A new algorithm has been developed and implemented for automated extraction of change objects from an elevation difference grid. This algorithm is built on the localized contour tree algorithm (Wu et al. 2015), which was originally developed for identifying surface depressions from topographic data and delineating their nested hierarchical structures. Our method is a combination of several computational steps: (1) generate an elevation difference grid; (2) create contours based on the elevation difference grid; (3) construct local contour trees; (4) simplify contour trees and identify critical contours as change objects; (5) derive semantic attributes for change objects; and (6) classify change objects into different types of damages in terms of their semantic properties based on the proposed ontology and taxonomy using the decision-tree method.

3.1. *Generating an elevation difference grid*

To illustrate our proposed method, we selected a small portion of the Bolivar Peninsula on the Texas Gulf Coast (location: 94° 29′ 40.912″ W, 29° 30′ 34.815″ N; see Figure 3(*a,b*)).

Assume that two surface DEMs have been acquired from sequential lidar surveys before and after a storm at times t_1 and t_2, respectively (e.g. Figure 3(c,d)). We also assume that the two DEMs are in raster format with the same spatial resolution and spatial extent and that they are referenced to a common map projection and datum. As data noise or errors in the DEM may lead to jagged, irregular, or fragmented contour lines (Wu et al. 2015), a 3×3 median filter (Wu, Lane, and Liu 2014) is applied to reduce data noise. Then the pre-storm DEM is subtracted from the post-storm DEM to create an elevation difference grid using Equation (1):

$$\Delta z_{i,j} = z_{i,j}^{t_2} - z_{i,j}^{t_1}, \qquad (1)$$

where $z_{i,j}^{t_1}$ is the elevation value of the pre-storm DEM at cell (i, j), and $z_{i,j}^{t_2}$ is the elevation value of the post-storm DEM at cell (i, j), and $\Delta z_{i,j}$ is the elevation difference
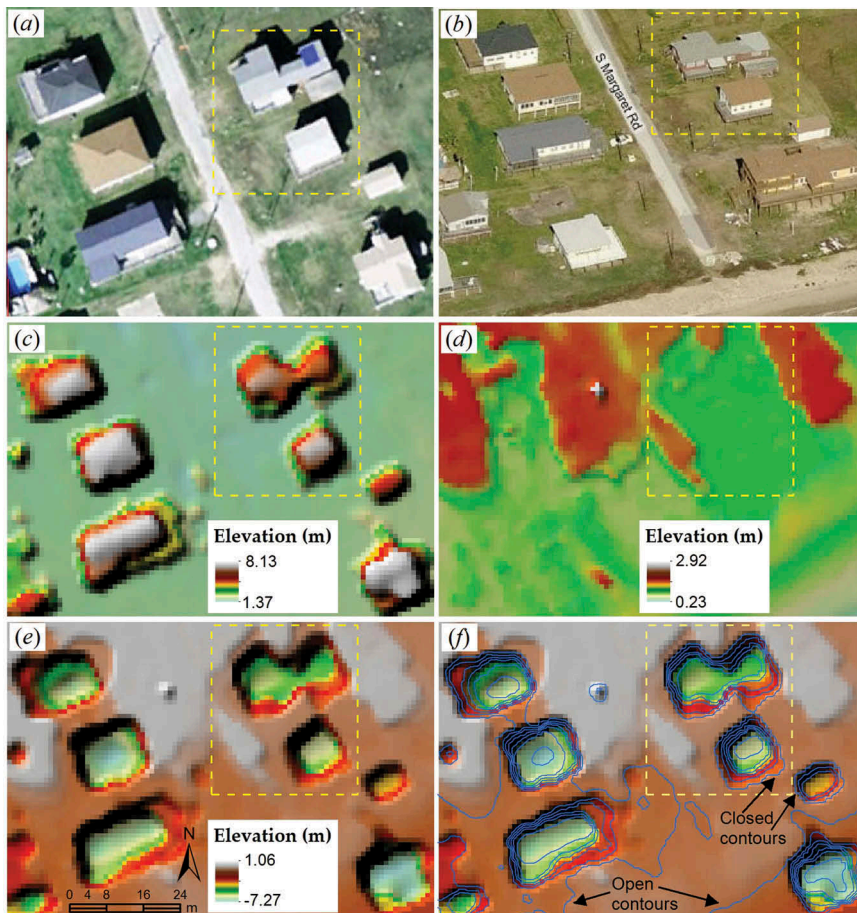

Figure 3. Generation of lidar elevation difference grid. The area shown is located in Bolivar Peninsula, Texas (94° 29′ 40.968″ W, 29° 30′ 34.906″ N): (a) Image from Google Earth; (b) image from Microsoft Bing map; (c) shaded relief map of pre-storm lidar DEM; (d) shaded relief map of post-storm lidar DEM; (e) shaded relief map of lidar elevation difference grid; and (f) contours overlain on shaded relief map.

between the post- and pre-storm DEM at cell (i, j). The difference grid removes topographic trend and only contains the change information that provides a quick visual effect of coastal change (e.g. Figure 3(e)). We consider a cell unchanged if its measured elevation difference is within the range of measurement error for a particular data set (say, ±0.25 m). Grid cells with negative difference values indicate places with sediment erosion or destroyed or damaged buildings, infrastructure, or trees, while cells with positive difference values indicate places with sediment accretion or relocation of buildings and trees. For convenience, we will refer to regions with negative elevation difference values as erosion objects and regions with positive elevation difference values as deposition objects.

3.2. Creating contours based on elevation difference grid

After generating the elevation difference grid, the highest value Δz_{max} and the lowest value Δz_{min} of this difference grid are identified (e.g. Figure 3(e)). To create contours on the elevation difference grid, two important parameters need to be determined: the base contour and the contour interval. The base contour is usually set to be the largest integer value less than or equal to the lowest value Δz_{min} of the difference grid. For example, the lowest value of the difference grid in Figure 3(e) is −7.27 m, thus the base contour can be set at −8.0 m. Contours are generated above the base contour as needed to cover the entire value range of the elevation difference grid based on a user-specified contour interval. The selection of a large contour interval will generate few contours and reduce computation time, but some small change objects would be missed as a consequence. A small contour interval will help to detect small change objects, but this will result in increased computation time. It should be noted that the selection of a contour interval for a set of DEMs may vary, depending on the process of interest and the scope of the study. Nonetheless, the contour interval should be larger than the vertical accuracy of the lidar-derived DEM.

Two types of contours are generated: open contours and closed contours (e.g. Figure 3(f)). An open contour has a starting and an ending point that intersect the study area boundary at different locations, while a closed contour is continuous without intersection with the boundary, forming a loop (Wu et al. 2015; Lindsay 2004). In a vector-based contour representation, change objects are represented as one or more closed contours in a concentric pattern (e.g. Figure 3(f)). Consequently, only closed contours are kept for further analysis while open contours are eliminated from further analysis, even though they may be indicative of important, landscape-scale changes. Erosion and deposition objects have distinctive contour patterns. An erosion object is indicated by a series of concentric closed contours with the inner contours having a lower elevation than their outer surrounding. Similarly, a deposition object has a concentric pattern of closed contours, but the elevation value decreases from inner contours to outer contours. Identification of erosion and deposition objects is analogous to the human visual interpretation of depressions and hills from topographical contour maps. The pit (lowest elevation value) of an erosion object is located inside the innermost closed contour. Likewise, the peak (highest elevation value) of a deposition object is located inside the innermost closed contour. The outermost closed contour of a change object approximates the spatial extent (boundary) of the change object.
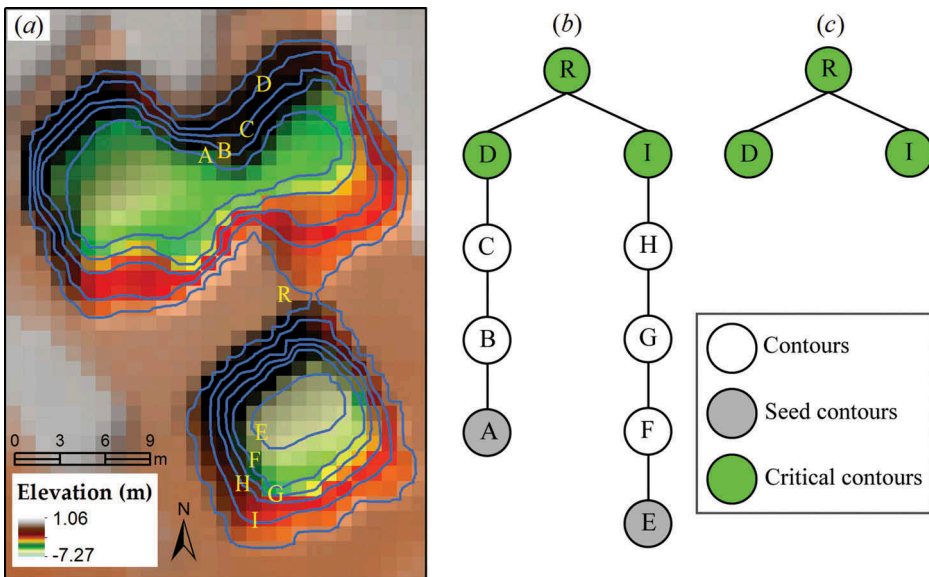
Figure 4. Illustration of a localized contour tree representation of change objects depicted in the dashed box in Figure 3: (*a*) contours overlain on shaded relief map; (*b*) the multi-branch contour tree representation of the corresponding composite change object in (*a*); and (*c*) the simplified contour tree representation.

It should be noted that both erosion and deposition objects may vary in size, depth, and shape. The composition and structure of change objects can be highly complex (Hahmann and Usery 2015). Some large, complex, change objects may contain smaller, nested change objects. In a contour map, the complex change objects are represented by the nested relationships of several sets of concentric closed contours. In Figure 4(*a*), for example, the region bounded by the outmost closed contour R contains two sets of concentric closed contours, which represent individual buildings (see Figure 3(*a*)).

3.3. Constructing local contour trees

A contour tree is a conceptual data structure for describing relationships among contours in continuous scalar fields based on the relationship between the critical points (local maxima, local minima and saddle points) where topological changes occur by the changes of contours (Kweon and Kanade 1994). The concept of contour trees was first proposed by Boyell et al. (1963) for representing spatial relations of contour lines where contours are mapped as nodes and interstitial spaces as links. There has been a great amount of work representing contour map as a tree structure, and various strategies have been proposed to transfer a contour map into a graph (Hahmann and Usery 2015; Qiao et al. 2005; Wu et al. 2015; Carr, Snoeyink, and van de Panne 2010; Carr, Snoeyink, and Axen 2003; van Kreveld et al. 1997; Wu 2011). Based on spatial relation theory and geometric characteristics of contours, Qiao et al. (2005) classified the spatial relations of contours into three categories: *k*th-order enclosure relation, parallel relation, and *k*th-order disjoint relation. In order to illustrate these different spatial relations of contours,

the example in Figure 4 was created. The contour tree in Figure 4(*b*) was generated by mapping the contours in Figure 4(*a*). The nodes in the tree represent contours, and the links between nodes represent adjacency and containment relationships between contours. Contour R has the highest elevation and directly or indirectly encloses all of the other contours. It has two immediate descendants of the same elevation, D and I, representing two branches of the tree. Contours D, C, and B have only one descendant each. Similarly, contours I, H, G, and F have one descendant each. Contours A and E have no descendants. In terms of spatial relations, contours D and I are the branches of R, which have a parallel relation. Contour D is the immediate descendant of R but is the parent node of C; it is defined that R first-order encloses D, and second-order encloses C. Contour C holds first-order disjoint relation with I, and holds second-order disjoint relation with H. In addition to the spatial relations between contours, a variety of spatial attributes can be calculated to quantify the shape characteristics of contours that are mapped as nodes in the contour tree, such as minimum distance to the parent node (MD), asymmetry (ASM), compactness index (CI), shape index (SHP), fractal dimension (FD), elongatedness (ELG), rectangularity (REC), ellipticity (ELP), and triangularity (TRI) (Liu et al. 2010). These attributes describe different aspects of the shape property, which provide a comprehensive shape description for contours.

From the perspective of graph theory, the hierarchical relationships of small change objects inside a larger composite change object constitute a tree. The outermost contour of the composite change object is the root of the tree, whereas the innermost closed contours are the leaf nodes of the tree. The corresponding contours of the leaf nodes are also called the 'seed contours', which are defined as the closed contours that do not enclose any other contours (Wu et al. 2015). Identification of seed contours is critical as they are used as the starting point to search outwards to minimize search time for establishing the contour tree graph. Compared with the global contour tree method (Wu 2011), the localized contour tree method is more effective and computationally efficient. Instead of creating a single global tree for an entire area, the localized contour tree algorithm constructs a forest of trees. Each tree represents one composite change object, and the number of trees in a forest represents the total number of composite change objects of the entire area.

3.4. *Identifying critical contours as change objects*

A simple change object constitutes a single-branch contour tree, while a composite change object is represented by a multi-branch contour tree (e.g. Figure 3(*f*)). In a contour tree, splitting and merging of node points represent changes in topology. For example, the corresponding contour tree of the composite change object shown in Figure 4(*a*) is a multi-branch tree. To explicitly represent the nested hierarchy of a composite change object, the contour tree is simplified by removing those nodes without topological change using a bottom-up searching strategy, starting from the leaf nodes (seed contours). Only those nodes with topological changes (immediately before merging) are kept in the simplification. It should be noted that the root node of a contour tree is always kept in the simplification because it represents the maximum boundary of a composite change object. After simplification, the multi-branch contour tree shown in Figure 4(*b*) is reduced to a smaller compact tree with only three nodes

(Figure 4(*c*)). The leaf nodes of the simplified contour tree represent the simple change objects at the first-level (e.g. nodes D and I in Figure 4(*c*)). The parent node of two or more leaf nodes in the simplified contour tree represents a composite change object at the second-level (e.g. nodes R in Figure 4(*c*)). The merging of a second-level change object with other first- or second-level change objects forms a more complex third-level change object. A composite change object may have more than one first-level simple change objects embedded within it. The simplified contour tree gives a clear representation of the nested hierarchical structure of a composite change object. The nested change objects can be merged to create multi-scale change objects.

Our experiments show that the localized contour tree algorithm overcomes the over-segmentation or under-segmentation biases that often come with a conventional single thresholding method and the fragmented artefact objects associated with the conventional morphological filtering method (Meinel and Neubert 2004). With the transition of the basic spatial units from grid cells to the change objects, the information and semantics are enriched in the form of identified, structured objects and associated attributes.

3.5. *Deriving semantic attributes for change objects*

Algorithms in computational geometry and computational topology have been used to derive a set of geometric, morphologic, and volumetric attributes (Figure 5) from lidar and imagery data for characterizing and quantifying change objects (Liu et al. 2010). The derived attributes include location, perimeter, area, compactness index, fractal dimension, elongatedness, orientation, surface slope and curvature variation, average elevation change, volume change, etc. normalized difference vegetation index (NDVI) can also be calculated for vegetation damage assessment by incorporating high-resolution colour infrared (CIR) aerial photographs. These attributes capture the fundamental aspects of morphological, geometric, shape, or thematic properties of change objects.
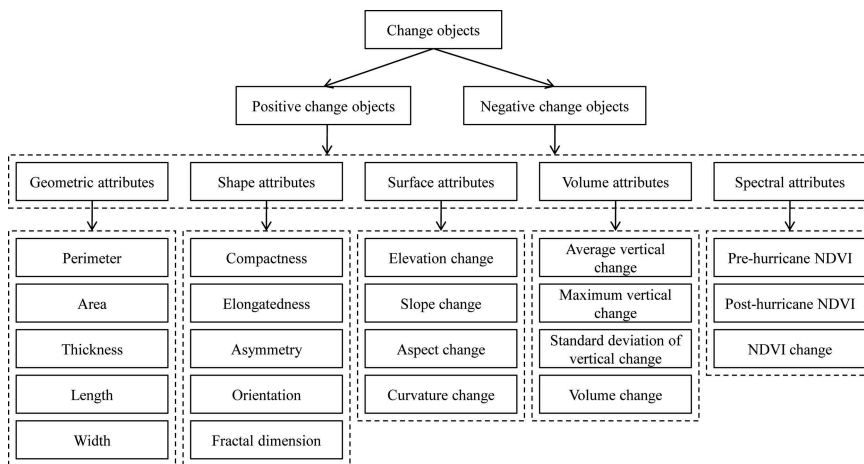

Figure 5. Derivation of semantic attributes of change objects.

4. Classification and damage assessment

As shown in Figure 2, the ontology-driven taxonomy provides the basic categories of coastal damages caused by storm hazards and the expected semantic properties and semantic relations of the damage categories. The change objects associated with building destruction, beach and sediment erosion and deposition, and vegetation damage have different spatial characteristics that are reflected in a certain range of attribute values. Change objects and their attributes have been computationally generated by using repeat lidar data and CIR aerial photographs. To map individual change objects to different damage categories, the categorization criteria and classification rules in terms of semantic properties and semantic relations must be formulated.

Based on prior domain knowledge and supervised learning with a training data set, the semantic properties and semantic relations expected for damage categories are digitally encoded as a set of explicit if–then rules. The decision-tree method C5.0 implemented in the open source R package C50 (Quinlan 2011; Kuhn et al. 2015) is employed to classify the change objects into different damage categories. C5.0 has been designed to have a scalability that scales well even where there are varying numbers of training examples and considerable numbers of attributes in substantial databases. As a nonparametric classifier, the decision-tree method makes no assumptions regarding the distribution model and its parameters for input attribute data (Liu and Wang 2008). Moreover, the decision-tree is easy to understand and modify, and the model can be expressed as a set of decision rules. Our decision-tree based classification comprises several operational steps: selecting training examples, choosing informative attributes, creating a decision tree, generating decision rules, classifying change objects and evaluating classification accuracy. The quantitative analysis of attribute values of individual change objects with reference to the if–then rules renders the capability of discriminating and classifying individual change objects into different damage classes: in the case of this application, building damage objects, sediment erosion objects, sediment deposition objects, and vegetation damage objects. After change objects are interpreted and classified into different damage categories, summary statistical attributes, including the number of destroyed buildings, total area of devastated trees, total area and volume of sediment erosion or deposition, can be calculated to depict the overall magnitude and spatial pattern of storm-induced coastal changes.

5. Implementation of contour tree-based change detection and object-based morphological change analysis software tools

In consideration of the extensive use of ArcGIS in both the geospatial research and emergency management communities, numerical algorithms for contour tree-based change detection and object-based morphological change analysis have been implemented as an ArcGIS toolbox, which is publicly available for download at http://spatial.binghamton.edu/software.html. The core algorithm components are implemented using Python programming language. The toolbox includes two tools: Object Extraction Tool and Attribute Derivation Tool. The Object Extraction Tool asks the user to provide two successive lidar DEMs that cover the same study area, and then executes the aforementioned procedures with user-specified parameters (base contour, contour interval, minimum area, minimum depth of change objects, etc.) automatically to create polygons of

change objects at different levels. It should be noted that the lidar DEMs should be pre-processed to have a common origin, the same map projection and be referenced to the same vertical datum. For the Attribute Derivation Tool, the user can select specific attributes to be computed. These attributes can be classified into three categories: planimetric attributes (centroid, perimeter, and area); shape attributes (compactness, elongatedness, fractal dimension, orientation, rectangularity, and ellipticity); and volumetric attributes (net volume change, and net volume change rate). The derived attributes are included in the feature attribute table of the object polygons, which are enclosed by identified critical contours. The computationally derived attributes provide comprehensively quantitative information of coastal morphological changes induced by hurricane or storm activities, which is unavailable in conventional pixel-based approach. All change objects and their associated computed attributes can be saved as ESRI Shapefile or Geodatabase format.

6. A case study

As shown above, the numerical algorithms have been implemented using ArcGIS and Python programming language to perform change object recognition and attribute derivation. The object-based analytical framework and algorithms were tested and evaluated with a case study that involves damage from the impact of Hurricane Ike on a portion of the Bolivar Peninsula on the Texas Gulf Coast. The spatial extent of the case study is 4500 m in the alongshore direction and 600 m in the cross-shore direction (Figure 6). The case study area includes settlements, beaches, foredunes, highway, trees and shrubs, grasses, geotubes, vehicles, etc. The geotubes are sediment-filled sleeves of geotextile fabric placed in a trench parallel to shore along the back beach or foredunes, preventing coastal properties from being undermined or damaged during storms and gradual shoreline retreat (Gibeaut et al. 2002).

Hurricane Ike made landfall as a strong category 2 storm with maximum sustained winds of 175 km hr^{-1} on September 13, 2008 (Doran et al. 2009), and its impacts have been widely studied (Sherman et al. 2013; Plant et al. 2010; Williams et al. 2009). The CIR aerial photographs (15-cm resolution) used in this analysis were acquired by the Texas General Land Office in August 2008 (pre-storm; Figure 6(b)) and in May 2009 (post-storm; Figure 6(c)), respectively. The pre-storm lidar data used in this analysis were acquired by the Texas Natural Resources Information System (TNRIS) in September 2006 (Figure 6(d)), and the post-storm lidar data were acquired by the Bureau of Economic Geology during December 12–13, 2008 (Figure 6(e)). The lidar data sets have a spatial resolution of 1 m and vertical accuracy of 10–20 cm. The lidar DEMs and aerial photos were projected to the Universal Transverse Mercator (UTM) zone 15 coordinate system, horizontally referenced to World Geodetic System (WGS) 84 ellipsoid. The elevation values are referenced to the orthometric North American Vertical Datum of 1988 (NAVD88). As shown in the shaded relief maps of lidar data (Figure 7), subtle and micro-morphological features such as buildings, beaches, dunes, roads, cars, vegetation, and geotubes can be resolved and recognized owing to the high density and vertical accuracy of the lidar measurements.

Due to registration errors, lidar data can be shifted and this shift needs to be identified and corrected if the data are used for assessment of topographic change. Systematic errors can be identified by comparing the lidar DEMs along pseudo-invariant features and
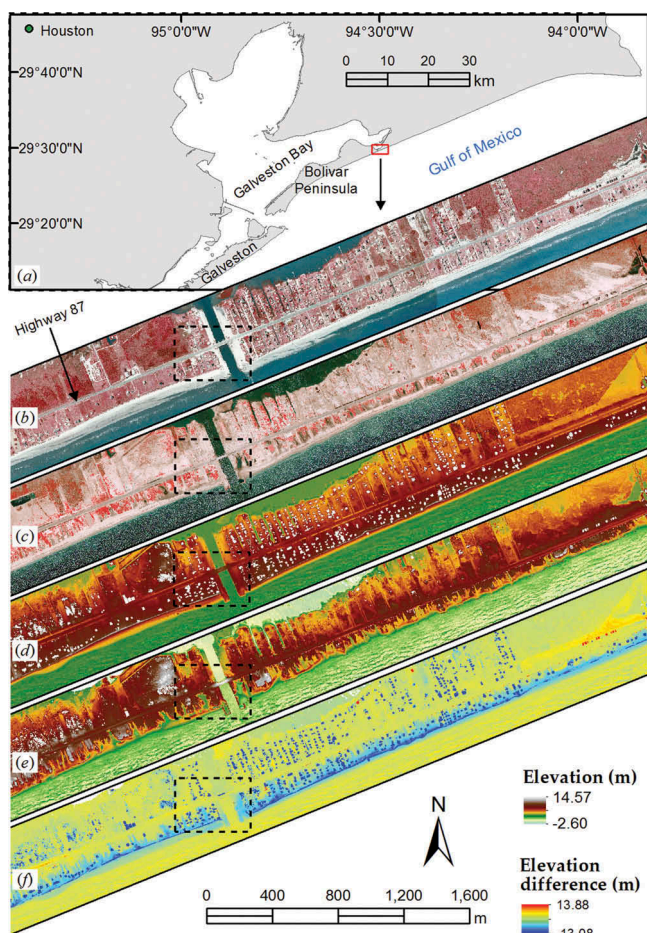
Figure 6. Data sets used for the case study: (*a*) location map of the Bolivar Peninsula on the Texas Gulf Coast; (*b*) pre-hurricane colour infrared aerial photographs acquired in August, 2008; (*c*) post-hurricane colour infrared aerial photographs acquired in May, 2009; (*d*) pre-hurricane lidar data acquired in September, 2006; (*e*) post-hurricane lidar data acquired in December, 2008; and (*f*) lidar elevation difference grid derived by subtracting pre- from post-hurricane lidar DEM. The dashed rectangles indicate the area shown in Figure 7.

geodetic benchmarks in open areas (Hardin et al. 2014a). In our case study area, the systematic errors were corrected using the centreline of Highway 87 (Figure 6(*b*)) under the assumption that the road surface did not change during the study time period and thus had a time-invariant elevation. As shown in Figure 8, the elevation values of the post-hurricane lidar DEM along the Highway 87 appear to be systematically higher than that of the pre-hurricane lidar DEM. The median and mean differences between the post- and pre-hurricane lidar DEMs are 5.3 and 5.5 cm, respectively. Although mean and median errors are often comparable, the median error is chosen in our case study area for its lower sensitivity to outliers. After removing the systematic errors of 5.3 cm from the post-hurricane DEM, the elevation difference grid is created by subtracting the pre-hurricane
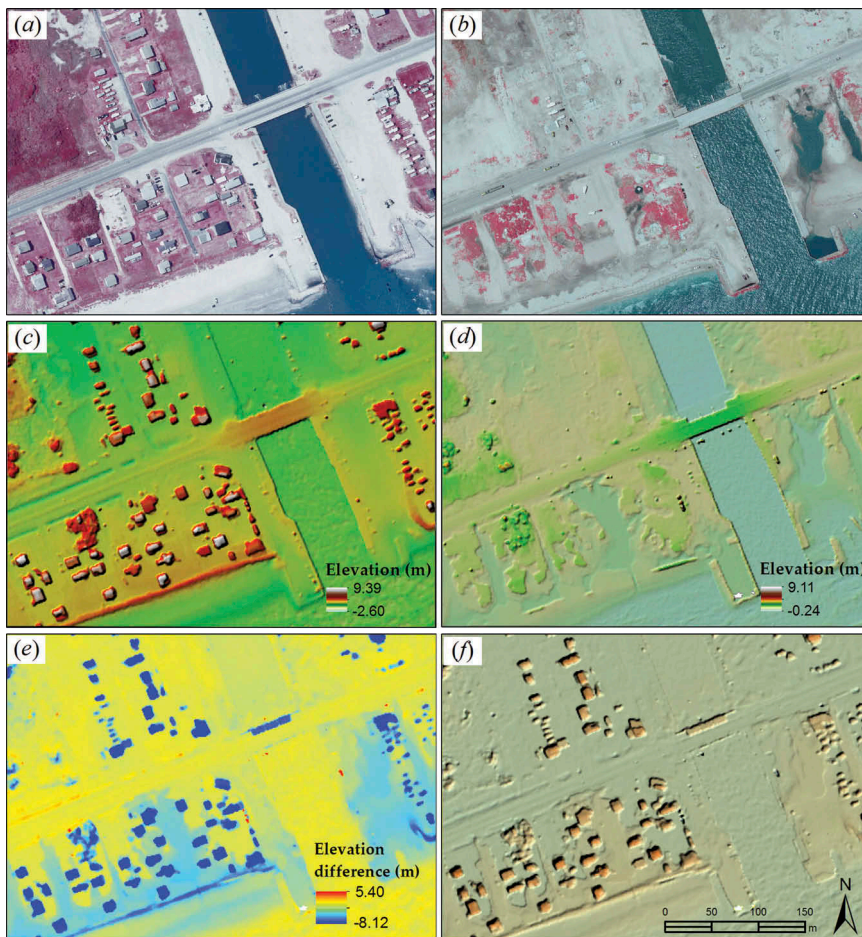
Figure 7. Coastal changes induced by Hurricane Ike near Rollover Pass, Texas as shown in the dashed box in Figure 6: (*a*) pre-hurricane colour infrared aerial photographs acquired in August 2008; (*b*) post-hurricane colour infrared aerial photographs acquired in May 2009; (*c*) shaded relief map of pre-hurricane lidar data acquired in September 2006; (*d*) shaded relief map of post-hurricane lidar data acquired in December 2008; (*e*) lidar elevation difference grid; and (*f*) shaded relief map of the lidar elevation difference grid.

DEM is from the post-hurricane DEM (Figure 6(*f*)), where sediment erosion zones and patches and destroyed buildings can be visually recognized.

By applying the localized contour tree method with specified parameters (base contour = −14 m; contour interval = 0.5 m; minimum area = 10 m^2; and minimum depth = 0.2 m), a series of change objects were numerically delineated as critical contours. Subsequently, geometric, shape, and volumetric attributes of these change objects were derived from lidar data and the NDVI image derived from the CIR aerial photographs. Base on the CIR aerial photographs, a shaded relief map of lidar DEM, and our prior knowledge, we assigned class labels to 52 change objects of various types. These labelled changes objects were used as training examples. Generally, the decision trees and rulesets constructed by C5.0 do not use all of the attributes. In our case,
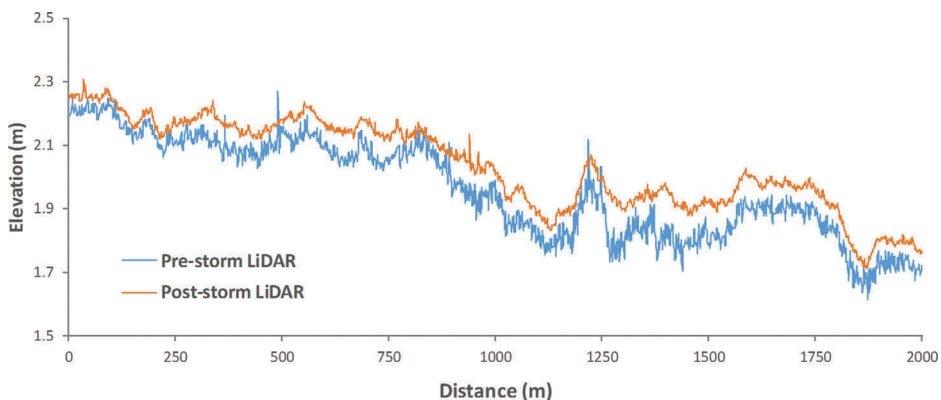
Figure 8. Systematic vertical offset between pre- and post-storm lidar DEMs.

although some spatial attributes may be useful for analysing the spatial pattern of damage induced by Hurricane Ike, they may not be helpful for discriminating different types of change object categories. By using the built-in winnowing function in C5.0 (Kuhn et al. 2015) to analyse the training examples, five attributes were selected for constructing the decision tree: pre-NDVI, pre-elevation, elevation difference, compactness, and elongatedness. The decision tree was then converted to rulesets that consist of a set of simple if–then rules (Figure 9), which were used as the classifier to predict the damage categories in the independent test dataset.

A portion of the classification results is shown in Figure 10. The classification accuracy is estimated to be as high as 95.9% (Table 1) by comparing with 590 reference objects developed from ground surveys and visual interpretation. It should be noted that conducting ground surveys and visually interpreting aerial photographs are time-consuming, labour-intensive, and spatially restrictive, which may delay response times and implementation of
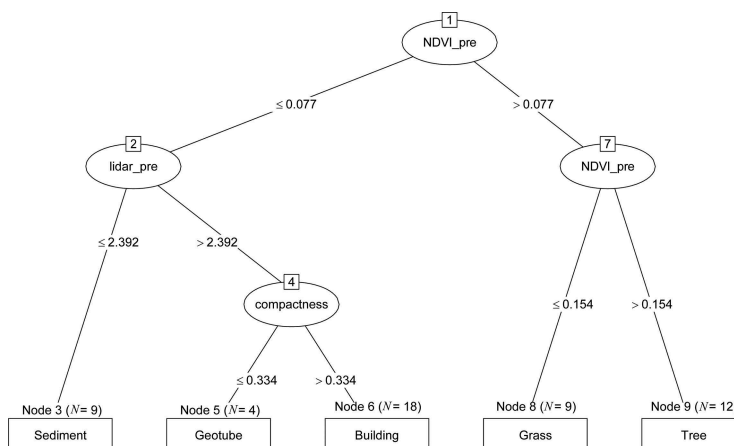

Figure 9. The decision tree constructed on the training dataset. 'NDVI_pre' represents the average pre-storm NDVI of each object. 'lidar_pre' represents the average pre-storm lidar elevation of each object. The numbers inside the squares indicate the node ID of non-terminal nodes in the decision tree. The numbers on the lines denote the decision rules for classifying objects.
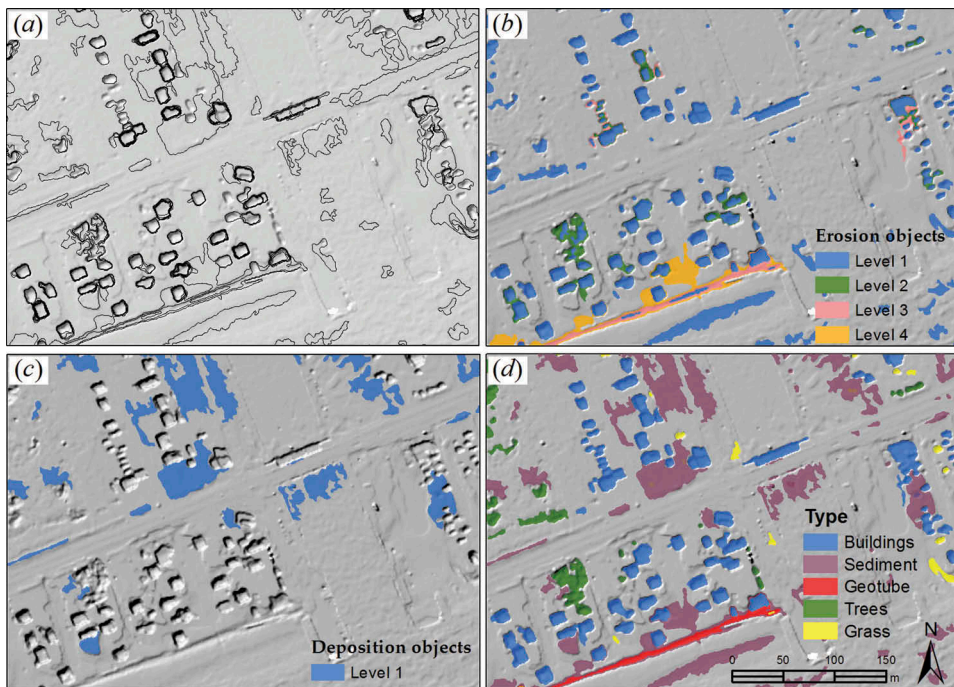
Figure 10. Samples of the classification result overlain on shaded relief maps. The area shown is the same as that shown in Figure 7: (*a*) contours with 0.5-m contour interval; (*b*) erosion objects derived using the localized contour tree method; (*c*) deposition objects derived using the localized contour tree method; and (*d*) classification of change objects using the decision-tree method.

Table 1. Classification error matrix with observed object types in the first column and classified object types under the respective headings. The diagonal elements in the error matrix represent the objects where the classification results agree with the referenced data. For example, 146 trees were observed, but 2 were identified as buildings and 6 were identified as grass.

Classification / Reference	Buildings	Trees	Grass	Geotubes	Sediment erosion	Sediment deposition	Row total
Buildings	124	2	0	0	4	0	130
Trees	2	138	6	0	0	0	146
Grass	0	4	88	0	2	0	94
Geotubes	0	0	0	20	0	0	20
Sediment erosion	2	0	2	0	92	0	96
Sediment deposition	0	0	0	0	0	104	104
Column total	128	144	96	20	98	104	590

corrective actions by coastal managers. Our proposed method provides an effective means for storm-induced coastal damage assessment in a rapid and timely manner for assisting in recovery efforts in the coastal communities affected. The classification map carries accurate quantitative information about the hurricane damage to buildings, beach and sand dunes, geotubes, and vegetation canopy. Within the case study area of 2.69 km^2, 77,900 m^2 of buildings, 1.8 km of geotubes, 6100 m^2 of trees and 16,400 m^2 of grass were destroyed. The total sediment erosion and deposition volumes are respectively 271,000 m^3 and 22,000 m^3. The shoreline was pushed landward by an average of 15.2 m.

7. Discussion and conclusions

This research presents a new algorithm to detect and delineate change objects from repeat lidar data sets. The algorithm is developed through a combination of elevation difference grid generation, local contour tree construction, critical contour identification, and semantic properties derivation. An ontology-driven, object-oriented analytical framework for storm-induced coastal damage assessment has been established, and algorithms for change object extraction and attribution have been implemented as software tools. The object-oriented method and software tool provide a powerful and effective means for reliable and accurate assessment of hazard damages in a rapid and timely fashion in order to support emergency response planning, rescue, and recovery activities.

The reliability and accuracy of the change objects detected by our proposed method may be affected by a number of factors. As demonstrated in the case study, our software tool for change object delineation requires two input data layers (pre- and post-storm lidar DEMs) and four user-defined parameters (base contour, contour interval, minimum size, minimum depth of change objects). Generally, the base contour is set as the nearest integer of the lowest value of the elevation difference grid derived by subtracting the pre-storm DEM from the post-storm DEM. The contour interval should set to be a value larger than the vertical accuracy of the lidar DEMs. The selection of a large contour interval will generate few contour lines and reduce computation time, but some shallow change objects might be missed during the contouring process. Conversely, a small contour interval can help to detect shallow change objects with a cost of increased computation time. As a general guideline, the minimum size of change objects should be at least two to three times larger than the spatial resolution of the lidar DEM, and the minimum depth should be larger than the vertical accuracy of the lidar DEM. As long as these recommended minimum requirements are met, the user is free to choose an optimal set of parameter values to detect and delineate change objects in a fully automated process.

As demonstrated with the case study, the object-oriented method proposed in this research overcomes the problems of conventional methods and results in high classification accuracy. The use of change objects as the basic spatial unit reduces the influence of data noise and enhances the reliability of extracted change and damage information. In contrast to grid cells in the field-based representation, objects are much better information carriers. The explicit object representation of change patches makes it possible to localize and depict damage hot spots. The concise and localized information about sediment erosion and deposition is useful for coastal managers to formulate intelligent decisions and policies for erosion control and coastal resource protection. The representation of erosion and deposition patches and zones as polygonal objects also facilitates overlay analysis in conjunction with other GIS data layers for exploring the causes and impacts of the volumetric and sediment changes.

Disclosure statement

Funding

ORCID

Qiusheng Wu 🔟 http://orcid.org/0000-0001-5437-4073
Bailang Yu 🔟 http://orcid.org/0000-0001-5628-0003

References

Agarwal, P. 2005. "Ontological Considerations in Giscience." *International Journal of Geographical Information Science* 19 (5): 501–536. doi:10.1080/13658810500032321.

Blaschke, T. 2010. "Object Based Image Analysis for Remote Sensing." *ISPRS Journal of Photogrammetry and Remote Sensing* 65 (1): 2–16. doi:10.1016/j.isprsjprs.2009.06.004.

Blaschke, T., G. J. Hay, M. Kelly, S. Lang, P. Hofmann, E. Addink, R. Q. Feitosa, et al. 2014. "Geographic Object-Based Image Analysis – Towards a New Paradigm." *ISPRS Journal of Photogrammetry and Remote Sensing* 87: 180–191. doi:10.1016/j.isprsjprs.2013.09.014.

Boyell, R. L., and H. Ruston. 1963. *Hybrid Techniques for Real-Time Radar Simulation*.

Carr, H., J. Snoeyink, and U. Axen. 2003. "Computing Contour Trees in All Dimensions." *Computational Geometry* 24 (2): 75–94. doi:10.1016/S0925-7721(02)00093-7.

Carr, H., J. Snoeyink, and V. D. P. Michiel. 2010. "Flexible Isosurfaces: Simplifying and Displaying Scalar Topology Using the Contour Tree." *Computational Geometry* 43 (1): 42–58. doi:10.1016/j.comgeo.2006.05.009.

Couclelis, H. 2010. "Ontologies of Geographic Information." *International Journal of Geographical Information Science* 24 (12): 1785–1809. doi:10.1080/13658816.2010.484392.

Doran, K. S., N. G. Plant, H. F. Stockdon, A. H. Sallenger, and K. A. Serafin. 2009. "Hurricane Ike: Observations and Analysis of Coastal Change." *US Geological Survey Open-File Report 1061*: 35.

Finkl, C. W., L. Benedet, and J. L. Andrews. 2005. "Interpretation of Seabed Geomorphology Based on Spatial Analysis of High-Density Airborne Laser Bathymetry." *Journal of Coastal Research* 21 (3): 501–514. doi:10.2112/05-756A.1.

Fonseca, F., C. Davis, and G. Camara. 2003. "Bridging Ontologies and Conceptual Schemas in Geographic Information Integration." *Geoinformatica* 7 (4): 355–378. doi:10.1023/A:1025573406389.

Gens, R. 2010. "Remote Sensing of Coastlines: Detection, Extraction and Monitoring." *International Journal of Remote Sensing* 31 (7): 1819–1836. doi:10.1080/01431160902926673.

Gibeaut, J. C., T. L. Hepner, R. Waldinger, J. R. Andrews, R. C. Smyth, and R. Gutierrez. 2002. *Geotubes Along the Gulf Shoreline of the Upper Texas Coast: Observations during 2001*. Austin, TX: University of Texas at Austin, Bureau of Economic Geology.

Goodchild, M. F. 1992. "Geographical Data Modeling." *Computers and Geosciences* 18 (4): 401–408. doi:10.1016/0098-3004(92)90069-4.

Hahmann, T., and E. L. Usery. 2015. "What Is in a Contour Map?" In *Spatial Information Theory*, edited by S. Fabrikant, M. Raubal, M. Bertolotto, C. Davies, S. Freundschuh, and S. Bell, 375–399, Springer International Publishing.

Hardin, E., H. Mitasova, L. Tateosian, and M. Overton. 2014a. "Processing Coastal Lidar Time Series." In *GIS-based Analysis of Coastal Lidar Time-Series*, 7–25. New York, NY: Springer.

Hardin, E., H. Mitasova, L. Tateosian, and M. Overton. 2014b. "Raster-Based Analysis." In *GIS-based Analysis of Coastal Lidar Time-Series*, 27–34. New York: Springer.

Heckmann, T., W. Schwanghart, and J. D. Phillips. 2015. "Graph Theory—Recent Developments of its Application in Geomorphology." *Geomorphology* 243: 130–146. doi:10.1016/j.geomorph.2014.12.024.

Houser, C., and S. Hamilton. 2009. "Sensitivity of Post-Hurricane Beach and Dune Recovery to Event Frequency." *Earth Surface Processes and Landforms* 34 (5): 613–628. doi:10.1002/esp.1730.

Kim, M., T. A. Warner, M. Madden, and D. S. Atkinson. 2011. "Multi-Scale GEOBIA with Very High Spatial Resolution Digital Aerial Imagery: Scale, Texture and Image Objects." *International Journal of Remote Sensing* 32 (10): 2825–2850. doi:10.1080/01431161003745608.

van Kreveld, M., R. van Oostrum, C. Bajaj, V. Pascucci, and D. Schikore. 1997. "Contour Trees and Small Seed Sets for Isosurface Traversal." In *Proceedings of the Thirteenth Annual Symposium on Computational Geometry*, 212–220. Nice, France: ACM.

Kuhn, M., S. Weston, N. Coulter, M. Culp, and R. Quinlan. 2015. "C5.0 Decision Trees and Rule-Based Models." *R Package Version 0.1.0-24*.

Kweon, I. S., and T. Kanade. 1994. "Extracting Topographic Terrain Features from Elevation Maps." *Computer Vision and Image Understanding* 59 (2): 171–182. doi:10.1006/cviu.1994.1013.

Lindsay, J. B. 2004. "Coping with Topographic Depression in Digital Terrain Analysis." PhD thesis, University of Western Ontario.

Liu, H., and L. Wang. 2008. "Mapping Detention Basins and Deriving Their Spatial Attributes from Airborne Lidar Data for Hydrological Applications." *Hydrological Processes* 22 (13): 2358–2369. doi:10.1002/hyp.6834.

Liu, H., L. Wang, D. Sherman, Y. Gao, and Q. Wu. 2010. "An Object-Based Conceptual Framework and Computational Method for Representing and Analyzing Coastal Morphological Changes." *International Journal of Geographical Information Science* 24 (7): 1015–1041. doi:10.1080/13658810903270569.

Liu, H., L. Wang, D. J. Sherman, W. Qiusheng, and S. Haibin. 2011. "Algorithmic Foundation and Software Tools for Extracting Shoreline Features from Remote Sensing Imagery and LiDAR Data." *Journal of Geographic Information System* 3 (2): 99–119. doi:10.4236/jgis.2011.32007.

Liu, Y., M. F. Goodchild, Q. Guo, Y. Tian, and L. Wu. 2008. "Towards a General Field Model and its Order in GIS." *International Journal of Geographical Information Science* 22 (6): 623–643. doi:10.1080/13658810701587727.

Mark, D., B. Smith, and B. Tversky. 1999. "Ontology and Geographic Objects: An Empirical Study of Cognitive Categorization." In *Spatial Information Theory. Cognitive and Computational Foundations of Geographic Information Science*, 747.

Meinel, G., and M. Neubert. 2004. "A Comparison of Segmentation Programs for High Resolution Remote Sensing Data." *International Archives of Photogrammetry and Remote Sensing* 35 (Part B): 1097–1105.

NOAA. 2013. "National Coastal Population Report, Population Trends from 1970 to 2020." In *NOAA State of the Coast Report Series*. Washington, DC: U.S. Department of Commerce.

Phillips, J. D., W. Schwanghart, and T. Heckmann. 2015. "Graph Theory in the Geosciences." *Earth-Science Reviews* 143: 147–160. doi:10.1016/j.earscirev.2015.02.002.

Plant, N. G., H. F. Stockdon, A. H. Sallenger, M. J. Turco, J. W. East, A. A. Taylor, and W. A. Shaffer. 2010. "Forecasting Hurricane Impact on Coastal Topography." *Eos, Transactions American Geophysical Union* 91 (7): 65–66. doi:10.1029/2010EO070001.

Qiao, C. F., J. Chen, R. L. Zhao, and J. Li. 2005. "Preliminary Studies on Contour Tree-Based Topographic Data Mining." Paper presented at the Proceedings of International Symposium on Spatio-temporal.

Quinlan, J. R. 2011. "See5: An Informal Tutorial."

Reif, M. K., J. M. Wozencraft, L. M. Dunkin, C. S. Sylvester, and C. L. Macon. 2013. "A Review of U.S. Army Corps of Engineers Airborne Coastal Mapping in the Great Lakes." *Journal of Great Lakes Research* 39 (S1): 194–204. doi:10.1016/j.jglr.2012.11.002.

Robertson, W. V., K. Zhang, and D. Whitman. 2007. "Hurricane-Induced Beach Change Derived from Airborne Laser Measurements near Panama City, Florida." *Marine Geology* 237 (3–4): 191–205. doi:10.1016/j.margeo.2006.11.003.

Rogers, L. J., L. J. Moore, E. B. Goldstein, C. J. Hein, J. Lorenzo-Trueba, and A. D. Ashton. 2015. "Anthropogenic Controls on Overwash Deposition: Evidence and Consequences." *Journal of Geophysical Research: Earth Surface* 120 (12): 2609–2624.

Sallenger, A. H., W. B. Krabill, R. N. Swift, J. Brock, J. List, M. Hansen, R. A. Holman, et al. 2003. "Evaluation of Airborne Topographic Lidar for Quantifying Beach Changes." *Journal of Coastal Research* 19 (1): 125–133.

Sallenger, A. H., H. F. Stockdon, L. Fauver, M. Hansen, D. Thompson, C. W. Wright, and J. Lillycrop. 2006. "Hurricanes 2004: An Overview of Their Characteristics and Coastal Change." *Estuaries and Coasts* 29 (6): 880–888. doi:10.1007/BF02798647.

Sherman, D. J., B. U. Hales, M. K. Potts, J. T. Ellis, H. Liu, and C. Houser. 2013. "Impacts of Hurricane Ike on the Beaches of the Bolivar Peninsula, TX, USA." *Geomorphology* 199: 62–81. doi:10.1016/j.geomorph.2013.06.011.

Trepanier, J. C., H. F. Needham, J. B. Elsner, and T. H. Jagger. 2015. "Combining Surge and Wind Risk from Hurricanes Using a Copula Model: An Example from Galveston, Texas." *The Professional Geographer* 67 (1): 52–61. doi:10.1080/00330124.2013.866437.

White, S. A., and Y. Wang. 2003. "Utilizing Dems Derived from LIDAR Data to Analyze Morphologic Change in the North Carolina Coastline." *Remote Sensing of Environment* 85 (1): 39–47. doi:10.1016/S0034-4257(02)00185-2.

Williams, A. M., R. A. Feagin, W. K. Smith, and N. L. Jackson. 2009. "Ecosystem Impacts of Hurricane Ike on Galveston Island and Bolivar Peninsula: Perspectives of the Coastal Barrier Island Network (CBIN)." *Shore & Beach* 77 (2): 71.

Wozencraft, J. M., and W. J. Lillycrop. 2003. "SHOALS Airborne Coastal Mapping: Past, Present, and Future." *Journal of Coastal Research* 207–215.

Wu, Q. 2011. "Object-Oriented Representation and Analysis of Coastal Changes for Hurricane-Induced Damage Assessment." Electronic thesis or diss., University of Cincinnati.

Wu, Q., C. Deng, and Z. Chen. 2016. "Automated Delineation of Karst Sinkholes from Lidar-Derived Digital Elevation Models." *Geomorphology* 266: 1–10. doi:10.1016/j.geomorph.2016.05.006.

Wu, Q., C. Lane, and H. Liu. 2014. "An Effective Method for Detecting Potential Woodland Vernal Pools Using High-Resolution LiDAR Data and Aerial Imagery." *Remote Sensing* 6 (11): 11444–11467. doi:10.3390/rs61111444.

Wu, Q., H. Liu, S. Wang, Y. Bailang, R. Beck, and K. Hinkel. 2015. "A Localized Contour Tree Method for Deriving Geometric and Topological Properties of Complex Surface Depressions Based on High-Resolution Topographical Data." *International Journal of Geographical Information Science* 29 (12): 2041–2060. doi:10.1080/13658816.2015.1038719.

Yu, B., H. Liu, W. Jianping, H. Yingjie, and L. Zhang. 2010. "Automated Derivation of Urban Building Density Information Using Airborne Lidar Data and Object-Based Method." *Landscape and Urban Planning* 98 (3–4): 210–219. doi:10.1016/j.landurbplan.2010.08.004.

Zhang, K., D. Whitman, S. Leatherman, and W. Robertson. 2005. "Quantification of Beach Changes Caused by Hurricane Floyd along Florida's Atlantic Coast Using Airborne Laser Surveys." *Journal of Coastal Research* 21 (1): 123–134. doi:10.2112/02057.1.